September 25th - 28th, 2017
INTERFACES
architecture . engineering . science IASS 2017 hamburg

*Proceedings of the IASS Annual Symposium 2017*
"Interfaces: architecture.engineering.science"
25 - 28th September, 2017, Hamburg, Germany
Annette Bögle, Manfred Grohmann (eds.)

# Ultra-Thin Composite Deployable Booms

Christophe LECLERC[a] *, Sergio PELLEGRINO[a]

[a] Graduate Aerospace Laboratories, California Institute of Technology
1200 E California Blvd, Pasadena, CA
* cleclerc@caltech.edu

## Abstract

The TRAC boom has many applications for spacecraft structures due to its efficient packaging. Reducing the thickness can extend the range of applications by enabling even tighter wrapping. A manufacturing process is proposed for ultra-thin TRAC booms with a total flange thickness of 71 μm. The mechanical behavior in both bending and torsion is studied through experiments. Increasing the flange opening angle is shown to greatly increase the bending stiffness around the Y axis, while increasing the bonded region width is shown to delay the appearance of local buckles and increase bending stiffness around the X axis.

**Keywords**: Deployable boom, Ultra-thin composites, Buckling, Rollable structure, Spacecraft structure, Thin shell structure

## Nomenclature

| | |
|---|---|
| EI | Bending stiffness |
| GJ | Torsional stiffness |
| r | Flange radius of curvature |
| t | Flange thickness |
| w | Bonded region width |
| θ | Flange opening angle |

## 1. Introduction

Deployable booms are key elements of many spacecraft architectures, allowing efficient packaging of systems that would otherwise be too large to fit inside a launch vehicle. One of their applications is to support large planar structures such as solar sails, antennas and photovoltaic arrays. This paper is focused on thin shell booms, examples of which are the Collapsible Tube Mast (CTM) and the Storable Tubular Extendable Member (STEM). They can be flattened and rolled into a spooled configuration. More recently, the Triangular Rollable And Collapsible (TRAC) boom has been developed by the Air Force Research Laboratory (Murphey and Banik [7]), and was first demonstrated in flight as part of the NanoSail-D mission in 2010 (Whorton *et al* [10]). It also has been considered for many other missions (Banik and Ardelean [1], Biddy and Svitek [3], McNutt *et al* [6]). The general architecture of the TRAC boom consists of two tape measures (flanges) bonded together along one edge, as shown in Figure 1. The important geometrical parameters are the flange radius $r$, the flange opening angle $\theta$, the bonded region width $w$, and the flange thickness $t$.

Recent research has shown that the TRAC boom compares favorably with the CTM and the STEM in terms of cross-sectional second moment of area to packaged height ratio, making it a promising candidate for space applications (Roybal *et al* [9]). Its open section leads to low torsional stiffness, which limits the extend of its uses. Most previous studies have considered metallic and relatively thick composite TRAC booms (Banik and Murphey [2]), limiting the range of applications. As the strain during packaging is related to the thickness, reducing this parameter would allow coiling around smaller hubs, enabling packaging of larger structures in smaller volumes.

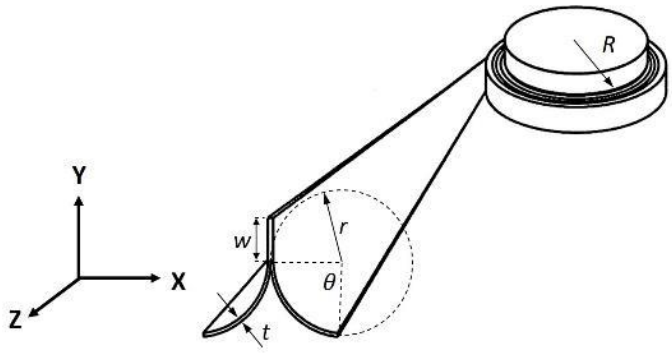


Figure 1: TRAC boom architecture (Modified from Banik and Murphy [2])

More recently, Murphey *et al* [8] have studied thinner TRAC booms, focusing on analytical and numerical prediction of the mechanical behavior. Also, Leclerc *et al* [5] and Fernandez [4] have studied ultra-thin TRAC booms, focusing on one specific geometry.

The present paper focuses on the characterization of three different geometries of ultra-thin TRAC booms, looking at the effects of varying the opening angle $\theta$ and the bonded region width $w$ on the mechanical behavior of the boom. First, a manufacturing process able to create the required boom architectures is introduced. Next, a method to measure, quantify and analyze the resulting shape of the manufactured booms is presented, followed by the experimental setups used for characterizing the mechanical behavior in both bending and torsion. Finally, the experimental results are analyzed and the performance of the different geometries are compared.

## 2. Manufacturing process

In order to reduce the mass and the packaged volume of the booms, ultra-thin prepreg composite materials are used for manufacturing. This material is provided as a uni-directional tape made of carbon fibers (Torayca T800) embedded in an epoxy resin (NTPT ThinPreg 402). It is manufactured by North Thin Ply Technology and has a dry areal density of 17 GSM, leading to a ply thickness of about 18 µm.

T800 carbon fibers have a diameter of about 5 µm, which coupled with the small thickness of this material leads to very few fibers across the thickness. Therefore, small imperfections such as fibers misalignment, uneven tow spreading, or gaps between fibers can significantly affect the shape and mechanical properties of the manufactured parts.

Manufacturing of TRAC booms has traditionally been done using a two-step process, where the flanges are fabricated first and then subsequently bonded together during a second step. A different approach is proposed where the two flanges are co-cured and bonded in a single step. Figure 2a shows the 3 part mold that is used. It consists of two U-shaped aluminum mandrels that form the TRAC shape, and a silicone plug that applies pressure inside the V-groove between the two mandrels. The carbon fiber layup is first draped over the molds. Then, the two aluminum mandrels are clamped together, pressing the composite material in between to create the bonded region. The silicone plug is added next, forming the curing configuration shown in Figure 2b. The resulting cured part, shown in Figure 2c is ultimately cut to create the desired TRAC boom (Figure 2d).

Three different geometries were manufactured, aiming to study the effect of the flange opening angle, $\theta$, and the bonded region width, $w$, on the mechanical properties. Table 1 summarizes the nominal geometrical parameters for each of the geometry, and Figure 3 shows the different cross sections. TRAC1 matches earlier studies (Leclerc *et al* [5]) and is used as a reference, while TRAC2 has a larger flange opening angle, and TRAC3 has a smaller bonded region width. The laminate used for all samples is $[0/90]_S$ in each flange, creating an 8-ply laminate in the bonded region.

Ten samples were manufactured: 4 of TRAC1, and 3 each of TRAC2 and TRAC3. The length of the samples is 540 mm.

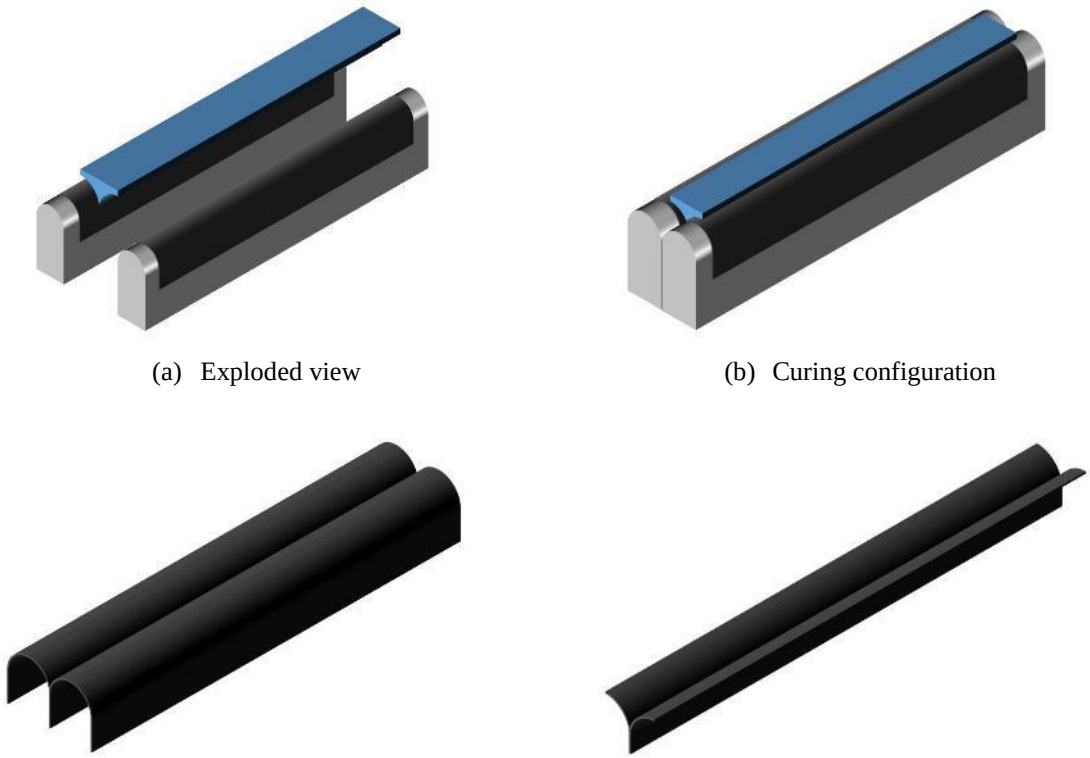

(a) Exploded view (b) Curing configuration

(c) Resulting cured part (d) Final part

Figure 2: Manufacturing process for TRAC boom

Table 1: TRAC booms geometrical parameters

| | r (mm) | θ (°) | w (mm) |
|---|---|---|---|
| TRAC1 | 10.6 | 105 | 8 |
| TRAC2 | 10.6 | 180 | 8 |
| TRAC3 | 10.6 | 105 | 4 |

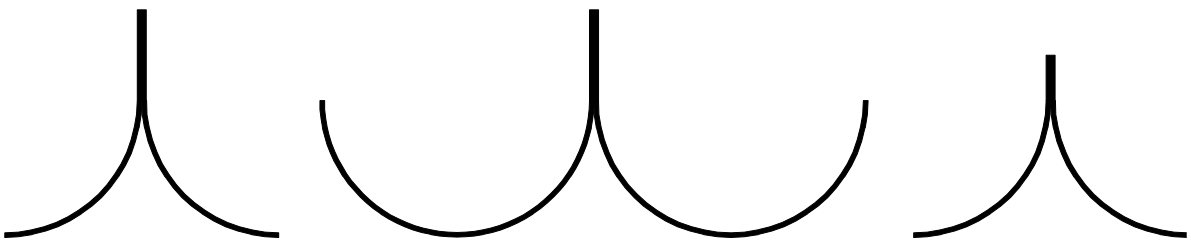

(a) TRAC1 (b) TRAC2 (c) TRAC3

Figure 3: Different TRAC boom geometries

## 3. Shape measurement

While the manufacturing process presented in Section 2 allows simple manufacturing of TRAC booms, residual stresses post-cure can significantly change the resulting shape. Indeed, the nominal mold curvature has a radius of 12.7 mm, but the composite parts spring in when removed from the mold, leading to a flange radius of 10.6 mm. Also, despite following the same nominally identical process in the manufacturing of all samples, their post-cure shape differed somewhat. To quantify this effect, a shape measurement method has been developed to accurately measure each sample and quantify the shape imperfections.

The first parameter that was measured is the flange thickness. It was obtained using micrographs taken by a microscope with calibrated optics (Nikon Eclipse LV150N). Three full cross section samples coming from different locations along the length of one boom were used, and thickness was measured at multiple locations along each of the cross sections. The samples were potted in clear epoxy, and the surface was polished until the desired finish. Figure 4 shows examples of micrographs for both a single flange (50X magnification) and the bonded region (20X magnification). The average thickness of a flange was estimated at 71 μm, and the thickness of the bonded region at 200 μm. Note that the thickness of the bonded region is almost three times the thickness of each flange.

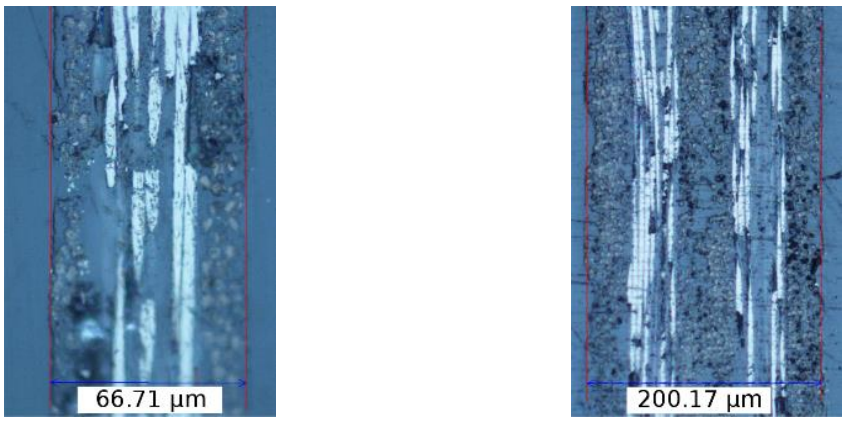


(a) Single flange (b) Bonded region

Figure 4: Micrographs of TRAC boom cross section

A Faro arm (Edge 14000) with a laser scanner attachment (ScanArm HD) was used to measure the shape of each sample. A point cloud was generated by the CAM2 Measure 10 software, and post processing was done using a Matlab script. The point cloud was first aligned with the TRAC boom coordinate systems shown in Figure 1. Then, boom cross sections were extracted at fixed interval along the booms. Next, the script carried out the following steps for each cross section:

1. The data points are split into two regions, one for each flange. Because the 3D scanner measures the surface, the bonded region is represented by two similar surfaces offset by the thickness, thus allowing the whole boom to be represented by two surfaces having a mostly constant thickness.
2. For each flange, the best fit circle is computed, and the radius and opening angles are extracted.
3. A known function is fitted to each region, and the full cross section is discretized.
4. The position of the centroid, second moments of area and orientation of the principal axes are computed using numerical integration.

The results at each cross section were used to compute the average radius and opening angle, the circularity of the flanges, the camber (out of plane deflection) and the torsion across the whole length. The point cloud was also analyzed to detect any local defects such as kinks at the flange edges.

In the case of the TRAC3 geometry, the residual stress post-cure coupled with the smaller bonded region led to shape instability. Indeed, the equilibrium shape showed an overall twist of 90° over the length of the sample. For only one of the samples with the TRAC3 geometry, a second stable configuration can be achieved, which removes almost all torsion, but shows a significant camber (up to 4.5 mm). Furthermore, when both ends are fully constrained from warping and twisting, only the straight configuration is stable. Due to this phenomenon, only one sample of the TRAC3 geometry could be used for further mechanical testing.

## 4. Experimental setups

Two different test setups were used to characterize the booms in bending and torsion. The interface between the samples and both test setup consisted of a 1.2 cm thick, laser-cut acrylic plate. A thin slot with the measured shape of the sample was filled with epoxy resin to allow efficient clamping of the sample. The centroid of the boom cross section was aligned with the center of the hole pattern used for attaching the acrylic plates to the test apparatus, ensuring the alignment between the samples and the rotation axis.

### 4.1. Bending experiment

The bending experimental setup (Figure 5) consisted of a gear system that control the in-plane rotation at each end of the sample. Hollow shafts instrumented with strain gauges measured the applied moments at both ends. Axial translation is kept free on one side, allowing the sample to shorten as it deforms. The interface on the apparatus has been designed to allow bending around the X or Y axes. Fine alignment of the sample with the experimental setup was done using shims in order to prevent any pre-stress being applied prior to the start of the experiment. Long rigid bars were attached at each end of the setup, to allow tracking of the rotation angle using photogrammetry.

Figure 5: Bending experimental setup

To test each sample, rotation was increased in small steps, keeping the moments equal at each end. After each increment, a picture was taken from above the sample. A Matlab script was used to locate the targets on the rigid bars and to compute the rotation angle $\alpha$, as shown in Figure 6. The moment was increased until buckling occurred. The bending stiffness was computed from

$$EI = \left(\frac{dM}{d\alpha}\right) L \tag{1}$$

where the derivative was obtained using a linear fit of the experimental data.

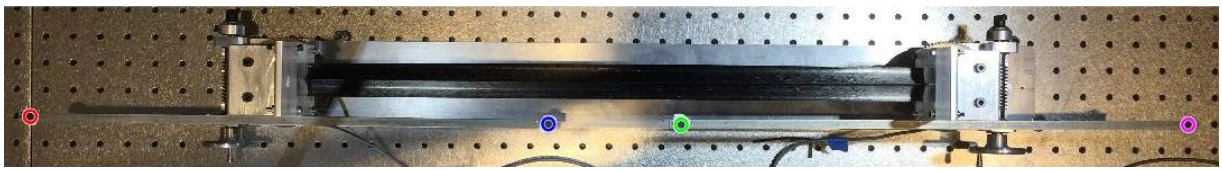

Figure 6: Example of a picture taken from above the experimental setup, with the 4 targets located and highlighted by the Matlab script

### 4.2. Torsion experiment

The torsion experimental setup (Figure 7) consisted of a fixed plate at one end, where the load was measured, and a movable end where the rotation was applied. The applied torque was measured using a 6 axis load cell (ATI Nano17 force/torque sensor). All force and moment components were measured by the load cell, to ensure that only pure torsion was applied to the sample. The rotation was enforced through a gearbox with a 60:1 reduction ratio (Ondrives P30-60), and the resulting twist angle $\beta$ was measured using a dial, giving a resolution of 0.06°. The axial displacement was kept free at the fixed end to account for reduction in length during torsion.

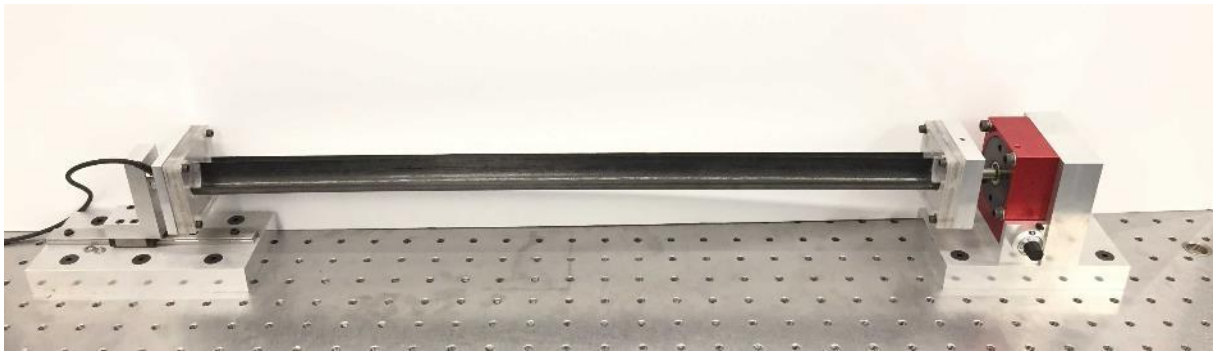

Figure 7: Torsion experimental setup

The torsional stiffness was computed from

$$GJ = \left(\frac{dM}{d\beta}\right) L \tag{2}$$

Similarly to the bending stiffness, the derivative was obtained through a linear regression of the experimental data. However, as the torsional behavior is non-linear, the fit was done over the first 5° of rotation.

## 5. Results and discussion

Three samples with TRAC1 and TRAC2 geometries were tested in bending and one sample only of each was tested in torsion. However, one TRAC1 configuration sample displayed premature failure in bending, so its results are excluded. Only one sample of TRAC3 was tested both in bending and in torsion. The results from the experiments are presented in Figure 8 and Figure 9. Table 2 summarizes the bending stiffness and torsional stiffness values, showing the average value from all experiments for each cross section. As each geometry corresponds to a different linear density, the properties are also normalized by the cross sectional area to facilitate comparison.

Table 2: Bending and torsional stiffness for all geometries

| | TRAC1 | TRAC2 | TRAC3 |
|---|---|---|---|
| $EI_X$ (N m$^2$) | 8.15 | 10.78 | 4.26 |
| $EI_Y$ (N m$^2$) | 3.32 | 56.07 | 2.40 |
| GJ (N m$^2$) | 0.0013 | 0.0380 | 0.0040 |
| $EI_X$ per unit cross section area (kN) | 2109 | 1872 | 1229 |
| $EI_Y$ per unit cross section area (kN) | 859 | 9735 | 692 |
| GJ per unit cross section area (kN) | 0.336 | 6.598 | 1.153 |

First, consider bending around the X axis (Figure 8a). A positive moment indicates that the bonded region is in compression for this loading case. Both TRAC1 and TRAC2 geometries show similar behavior, where a positive loading leads to a bi-linear response while a negative loading leads to a linear response. The bi-linear response is due to the buckling of the bonded region. After reaching a certain compression level, the bonded region starts to deform into a sinusoidal shape along the full length, leading to a decrease in stiffness. Global buckling of the structure occurs when the bonded region snaps from a global sinusoidal shape to a local, single sinusoid of larger amplitude. Due to its much smaller bonded region, TRAC3 quickly reaches local buckling when a positive moment is applied, leading to a smaller bending stiffness. Note that for this loading case, TRAC1 and TRAC2 have very similar normalized bending stiffness (11% difference).

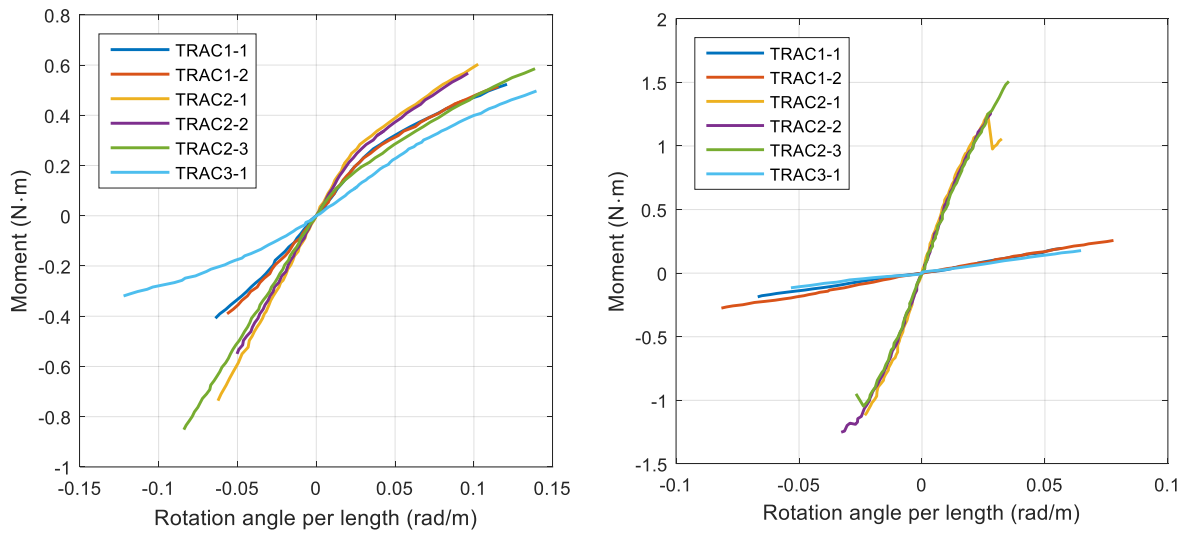


(a) Bending around X

(b) bending around Y

Figure 8: Comparison of bending results for the 3 geometries

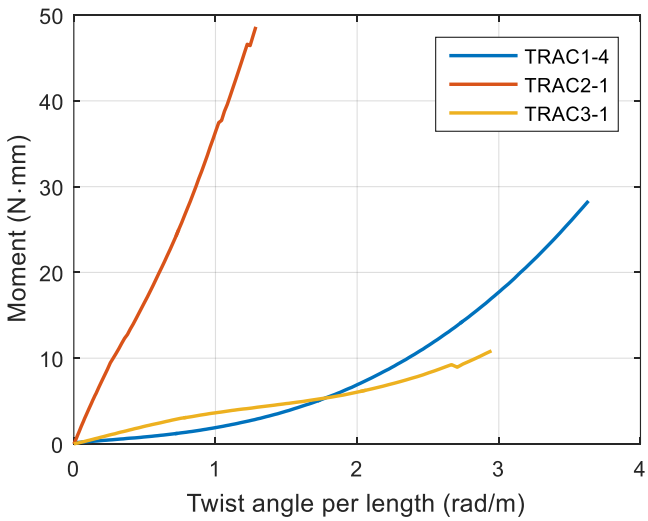


Figure 9: Comparison of torsion results for the 3 geometries

In the case of bending around the Y axis (Figure 8b), the behavior displayed by TRAC1 and TRAC3 is similar. TRAC2 begins to soften after reaching a moment of about 0.5 N·m, corresponding to the appearance of small local buckles along the edge of the flange in compression. Leclerc *et al* [5] have shown that premature buckling of the flanges in the case of the TRAC1 geometry leads to a decrease in stiffness of 60%. While the TRAC3 geometry behaves similarly, the larger opening angle of TRAC2 removes this effect by stabilizing the most highly compressed part of the cross-section, which is no longer a free edge.

These results indicate that the bonded region has a significant impact on the behavior in bending around X, but limited impact on bending around Y. Increasing the flange opening angle greatly improves the stiffness around Y, increasing it by a factor of 11 when normalized and compared with TRAC1.

Due to its thin shell open cross section, TRAC booms present very low torsional stiffness. Increasing the opening angle leads to a twentyfold increase in normalized stiffness, as shown in Figure 9. A key difference between TRAC1 and TRAC2 is that the moment increases quadratically with the twist for the former, and linearly for the latter. While this phenomenon is not currently fully understood, local buckling of the flange edges for the TRAC2 geometry were observed during experiments. This softening due to buckling could partially offset the increase in stiffness seen for TRAC1. Because of the previously observed bi-stable configuration in torsion of the TRAC3 geometry, results for this specific cross section cannot be reliably compared with TRAC1 and TRAC2. However, this could explained the softening effect seen in Figure 9.

## 6. Conclusion

Reducing the thickness of coilable booms can significantly decrease the packaged radius, enabling new applications. The present study explored TRAC booms made of ultra-thin carbon fiber-epoxy prepregs. A manufacturing process was proposed, yielding 0.54 m long booms with a flange thickness of 71 μm. Due to thermal effects during curing process, and defects inherent to ultra-thin composite materials, the post-cure shapes can differ from the desired shape. Hence, a measurement technique to assess shape variations was described. Finally, bending and torsion experiments were conducted on samples with three different cross sections. Increasing the flange opening angle from 105° to 180° greatly improved the bending stiffness around the Y axis and the torsional stiffness, while having negligible impact on the bending stiffness around X. Decreasing the bonded region width from 8 mm to 4 mm was shown to decrease bending stiffness around X by causing early localized buckles, while having no significant impact on bending stiffness around Y.

## Acknowledgements

The authors would like to acknowledge financial support from the Northrop Grumman Corporation, the Natural Science and Engineering Research Council of Canada and the Keck Institute for Space Studies.

## References

[1] Banik J.A. and Ardelean E.V., "Verification of a Retractable Solar Sail in a Thermal-Vacuum Environment", in *Proceedings of 51st AIAA/ASME/ASCE/AHS/ASC Structures, Structural Dynamics, and Materials Conference*, Orlando, FL, 2010, AIAA 2010-2585.

[2] Banik J.A. and Murphey T.W., "Performance Validation of the Triangular Rollable and Collapsible Mast", in *Proceedings of 24th Annual AIAA/USU Conference on Small Satellites*, Logan, UT, 2010, SSC10-II-1.

[3] Biddy C. and Svitek T., "LightSail-1 Solar Sail Design and Qualification", in *Proceedings of 41st Aerospace Mechanisms Symposium*, 2012.

[4] Fernandez J.M., "Advanced Deployable Shell-Based Composite Booms for Small Satellite Structural Applications Including Solar Sails", in *Proceedings of 4th International Symposium on Solar Sailing*, Kyoto, Japan, 2017.

[5] Leclerc C., Wilson L., Bessa M.A. and Pellegrino S., "Characterization of Ultra-Thin Composite Triangular Rollable and Collapsible Booms", in *Proceedings of 4th AIAA Spacecraft Structure Conference*, Grapevine, TX, 2017, AIAA 2017-0172.

[6] McNutt L., Johnson L., Clardy D., Castillo-Rogez J., Frick A. and Jones L., "Near-Earth Asteroid Scout", *AIAA Space 2014 Conference and Exposition*, San Diego, CA, 2014, AIAA 2014-4435.

[7] Murphey T.W. and Banik J.A., *Triangular rollable and collapsible boom*, March 1 2011, US Patent 7,895,795.

[8] Murphey TW, Turse D.A. and Adams L.G., "TRAC™ Boom Structural Mechanics", in *Proceedings of 4th AIAA Spacecraft Structure Conference*, Grapevine, TX, 2017, AIAA 2017-0171.

[9] Roybal F.A., Banik J.A. and Murphey T.W., "Development of an Elastically Deployable Boom for Tensioned Planar Structures", in *Proceedings of 48th AIAA/ASME/ASCE/AHS/ASC Structures, Structural Dynamics, and Materials Conference*, Honolulu, HI, 2007, AIAA 2007-1838.

[10] Whorton M., Heaton A., Pinson R., Laue G. and Adams C., "Nanosail-D: The First Flight Demonstration of Solar Sails for Nanosatellites", *in 22nd AIAA/USU Conference on Small Satellites*, Logan, UT, 2008, SSC08-X-1.